

Efficient Iterative Proximal Variational Inference Motion Planning

Zinuo Chang^{a,1}, Hongzhe Yu^{b,1,*}, Patricio Vela^a, Yongxin Chen^b

^a*School of Electrical and Computer Engineering, Georgia Institute of Technology, Atlanta, GA*

^b*School of Aerospace Engineering, Georgia Institute of Technology, Atlanta, GA*

Abstract

Motion planning under uncertainty can be cast as a stochastic optimal control problem where the optimal posterior distribution has an explicit form. To approximate this posterior, this work frames an optimization problem in the space of Gaussian distributions by solving a Variational Inference (VI) in the path distribution space. For linear-Gaussian stochastic dynamics, we propose a proximal algorithm to solve for an optimal Gaussian proposal iteratively. The computational bottleneck is evaluating the gradients with respect to the proposal over a dense trajectory. We exploit the sparse motion planning factor graph and Gaussian Belief Propagation (GBP), allowing for parallel computing of these gradients on Graphics Processing Units (GPUs). We term the novel paradigm as the Parallel Gaussian Variational Inference Motion Planning (P-GVIMP). Building on the efficient algorithm for linear Gaussian systems, we then propose an iterative paradigm based on Statistical Linear Regression (SLR) techniques to solve motion planning for nonlinear stochastic systems, where the P-GVIMP serves as a sub-routine for the linearized time-varying system. We validate the proposed framework on various robotic systems, demonstrating significant speed acceleration achieved by leveraging parallel computation and successful planning solutions for nonlinear systems under uncertainty. An open-sourced implementation is presented at <https://github.com/hzyu17/VIMP>.

1. Introduction

Motion Planning is one core decision-making component in autonomous robotic systems [1, 2]. Given an environment, a start configuration and a goal configuration, a motion planner computes a trajectory connecting the two configurations. The trajectory optimization paradigm [3, 4] formulates the motion planning problem as an optimization over all admissible trajectories with dynamics and environment constraints. An ‘optimal’ plan can be obtained by solving the optimization program by minimizing certain optimality indexes, such as time consumption and control energy.

Uncertainties such as sensing [5], actuation noises, and external disturbances [6] arise and affect the quality of the motion plans in the execution phase. To reduce their impacts, motion planning under uncertainties takes into account the uncertainties in the planning phase in their formulations [7]. Stochastic optimal control and probabilistic robotics [8, 9] provide a principled framework to address this problem, where noise is explicitly modeled in robot dynamics, and a statistical optimality index is minimized over the trajectory distribution space.

Gaussian Process Motion Planning (GPMP) paradigm [10, 11] used the linear SDE dynamics model to formulate motion planning problems as probability inference, where the optimal solution is formulated as a posterior probability. The objective in GPMP is solving a trajectory that maximizes this posterior.

The solution obtained from GPMP is still deterministic. Variational Inference (VI) [12, 13] formulates the inference problem into an optimization by minimizing the Kullback–Leibler (KL) divergence between a proposal distribution and the target posterior. VI has been applied to solve for a trajectory distribution in the planning-as-inference formulation [14, 15, 16, 17]. Gaussian Variational Inference Motion Planning (GVIMP) [14, 15] showed satisfying performances in challenging tasks such as planning through narrow gaps [18]. The GVIMP formulation is related to entropy-maximized motion planning and reinforcement learning [19, 20, 21, 22].

Introducing distributional variables increases the dimension of the problem. Fortunately, in motion planning problems, the underlying probabilistic graph enjoys a sparsity pattern [23, 11] which is leveraged in algorithm designs to factorize the target posterior and reduce the time complexity [24, 15]. In this work, we study the proximal point GVI algorithm [25, 26] over the motion planning factor graph, where we show the updates in explicit form and that these gradient computations can be distributed onto the factor levels over the factor graph.

In terms of computation efficiency, similar to deterministic trajectory optimization paradigms [10, 11, 4], the collision-checking step of the algorithm on a dense trajectory is computationally demanding in GVIMP and represents the computational bottleneck [15]. In this work, we further leverage the sparse factor graph to distribute the collision-checking computations in parallel on a GPU. We also deployed the Gaussian Belief Propagation (GBP) [27, 28] algorithm for efficient marginal covariance computation. We term the algorithm the Parallel Gaussian Variational Inference Motion Planning (PGVIMP).

Most existing planning-as-inference paradigms [11, 29, 14]

*Corresponding author.

Email address: hzyu419@gatech.edu (Hongzhe Yu)

¹These authors contributed equally to this work.

assume linear SDE as the underlying dynamics. Different from these works, we solve the problem for *nonlinear* stochastic differential equations (SDEs) [30], where we make the standard Gaussian transition assumption widely used in robotics applications [31, 32]. We then perform the Statistic Linear Regression (SLR) iteratively to obtain a linear time-varying (LTV) system in each iteration and perform PGVIMP on the obtained LTV system. This process integrates the sequential Bayesian principles into the GVIMP framework for motion planning tasks.

Related Works.

(a) *Proximal Variational Inference.* The proximal point algorithm and its stochastic version were first proposed in [25], where the KL-divergence was used as the proximal operator. The connection between the proximal-point and natural gradient descent algorithms was pointed out in [25, 13]. [26] generalized the proximal point variational inference algorithms by replacing the proximal term with general divergence functions. Recently, [33] proposed a proximal gradient algorithm by decomposing the KL-divergence objective into a potential and an entropy term. The above algorithms were applied directly to the joint posterior over all the variables without considering the factor graph structure of the posterior.

(b) *Iterative approximations for nonlinear stochastic processes.* The techniques based on iterative linearization to approximate nonlinear stochastic processes originated in the nonlinear state estimation literature. Related works are the Extended Kalman Filter (EKF), which leverages the Taylor approximation [34], statistical approximations based on moment matching [34], Laplace approximation [35], and cubature approximation [36]. In [37] the authors first introduced the use of Gauss-Hermite quadrature methods in the nonlinear estimation problems. To the best of the author’s knowledge, this work is the first to solve nonlinear planning problems by integrating iterative approximations and variational inference.

(c) *Parallel Motion Planning.* Parallelism and GPU acceleration have been applied to motion planners. The works [38, 39, 40, 41] proposed GPU-accelerated sampling-based motion planning algorithms. [42, 43] used GPU for fast collision-checking, which is a bottleneck in motion planning. The authors of [44] applied GPU acceleration in model predictive control algorithm for online control of high-DOF robotic systems. All these works dealt with collision-checking for deterministic states, while in our work, we solve collision-checking in a probabilistic sense, i.e., we compute an expected collision cost with respect to a proposal distribution over a dense trajectory.

In this work, we leverage this sparse factor and the parallel computing on GPUs to accelerate the computation of two key components in the GVI motion planning paradigm: the parallel computation of the collision likelihood and the computation of marginal covariances over the sparse factor graph.

Key Contributions. The contributions of this work are: (1) We proposed a KL-proximal variational inference algorithm for robot motion planning, where we show that the proximal gradient computations in the paradigm can be parallelized by leveraging a splitting structure and the underlying sparse factor graph; (2) A parallel computation implementation on GPU of the KL-proximal algorithms is proposed, where we lever-

aged parallel computation of the collision costs and Gaussian Belief Propagation (GBP) to compute marginal covariances efficiently; (3) We propose a sequential statistical linearization scheme for motion planning of nonlinear dynamical systems, where we use the parallel KL-proximal algorithm for linear systems as a submodule at each outer iteration.

Planning results are demonstrated on various robot models and comparison studies have been conducted to demonstrate the efficiency improvement.

This work builds upon the author’s prior work [14, 15], where we addressed the issue of computation efficiency, explored the KL-proximal GVI algorithm in the path distribution space for motion planning, and the applicability of the GVIMP approach to nonlinear dynamics.

This paper is organized as follows. Section 2 introduces the background knowledge. Section 3 introduces the KL-proximal GVI algorithm and its structure for motion planning problems. Section 4 introduces the sparse motion planning factor graph and marginal gradient updates for the KL-proximal algorithm. Section 5 introduces the iterative PGVIMP algorithm for nonlinear systems. The proposed framework is illustrated in Section 7 through numerical experiments, followed by a conclusion in Section 8.

2. Variational Inference Motion Planning (VIMP)

This section introduces some important preliminary knowledge of this paper, including motion planning under uncertainty and variational inference motion planning.

2.1. Planning under Uncertainties as Stochastic Control

We solve the motion planning under uncertainties using the stochastic control framework. For the *nonlinear* process

$$dX_t = f(X_t, u_t)dt + g_t(X_t)dW_t, \quad (1)$$

we minimize the following objective

$$\min_{X(\cdot), u(\cdot)} \mathcal{J} \triangleq \mathbb{E} \left\{ \int_0^T \frac{1}{2} \|u_t\|^2 + V(X_t)dt + \Psi_T(X_T) \right\} \quad (2)$$

where the running cost consists of a state-related cost $\int_0^T V(X_t)dt$, a control energy cost $\int_0^T \frac{1}{2} \|u_t\|^2 dt$, and $\Psi_T(x_T)$ is a state terminal cost. The state costs regulate the desired behaviors, such as collision avoidance. Controlling energy costs promotes a minimum energy consumption strategy for the robot to achieve the above goals. The *prior* process associated with the process (1) is defined by letting $u_t \equiv 0$, resulting in the process

$$dX_t = f_0(X_t)dt + g_t(X_t)dW_t. \quad (3)$$

Gaussian assumptions. The state distribution of system (1) follows the Fokker-Planck (FPK) equations, leading to non-Gaussian distributions for the states under the nonlinearity (1). It is hard to solve the FPK for general nonlinearities [], and Gaussian assumptions are one popular approximation assumption in the robotics applications, especially in the filtering and estimation [32, 31].

2.2. Gaussian Variational Inference Motion Planning (GVIMP)

Problem (2) admits an equivalent path distribution control formulation that will be introduced in this section.

(a) *Control-inference duality.* Denote the measure induced by the controlled linear process (7) as \mathbb{Q} , and the measure induced by the prior process (3) as \mathbb{P} . By Girsanov's theorem [45], the following objective is equivalent to (2) [15, 46]

$$\begin{aligned} \mathcal{J} &= \mathbb{E}_{\mathbb{Q}}[\log \frac{d\mathbb{Q}}{d\mathbb{P}} + \mathcal{V}] \propto \mathbb{E}_{\mathbb{Q}}[\log d\mathbb{Q} - \log \frac{e^{-\mathcal{V}} d\mathbb{P}}{\mathbb{E}_{\mathbb{P}}[e^{-\mathcal{V}}]}] \\ &= \text{KL}(\mathbb{Q} \parallel \mathbb{Q}^*), \end{aligned} \quad (4)$$

where the cost-related functional $\mathcal{V} \triangleq \int_0^T V(X_t)dt + \Psi_T(X_T)$, and the measure \mathbb{Q}^* is defined as

$$d\mathbb{Q}^* \triangleq \frac{e^{-\mathcal{V}}}{\mathbb{E}_{\mathbb{P}}[e^{-\mathcal{V}}]} d\mathbb{P} \propto e^{-\mathcal{V}} d\mathbb{P}. \quad (5)$$

Path space Variational Inference is formulated as [10, 15]

$$q^* = \arg \min_{q_\theta \in \mathcal{Q}} \text{KL}(q_\theta \parallel \mathbb{Q}^*) \quad (6)$$

where $\mathcal{Q} \triangleq \{q_\theta : q_\theta \sim \mathcal{N}(\mu_\theta, \Sigma_\theta)\}$ consists of the parameterized proposal Gaussian distributions.

(b) *Linear-Gaussian System Case.* When the stochastic process (1) reduces to linear time-varying stochastic system

$$dX_t = (A_t X_t + a_t + B_t u_t)dt + B_t dW_t, \quad (7)$$

the associated prior process is

$$dX_t = (A_t X_t + a_t)dt + B_t dW_t. \quad (8)$$

Consider the above KL-minimization problem (4) with the time discretization

$$\mathbf{t} \triangleq [t_0, \dots, t_N], \quad t_0 = 0, \quad t_N = T. \quad (9)$$

For linear Gaussian prior dynamics (8), the discrete-time path distribution $d\mathbb{P}$ over \mathbf{t} is a Gaussian distribution $\mathbf{X} \sim \mathcal{N}(\boldsymbol{\mu}, \mathbf{K})$. The discrete-time cost factor $e^{-\mathcal{V}}$ is defined as

$$e^{-\mathcal{V}} = e^{-\int_0^T V(X_t)dt + \Psi_T} \approx e^{-\sum_{i=0}^N V(X_i) \times \Delta t},$$

then the un-normalized discrete-time optimal distribution to the problem (5) and is defined as

$$\mathbb{Q}^*(\mathbf{X}) \propto e^{-\frac{1}{2}\|\mathbf{X} - \boldsymbol{\mu}\|_{\mathbf{K}^{-1}}^2 - \sum_{i=0}^N V(X_i)} \triangleq \tilde{q}^*(\mathbf{X}). \quad (10)$$

Under this discretization, the inference problem (6) becomes

$$\min_{\mu_\theta, \Sigma_\theta} \mathbb{E}_{q_\theta \sim \mathcal{N}(\mu_\theta, \Sigma_\theta)} [V(\mathbf{X})] + \text{KL}(q_\theta \parallel \mathcal{N}(\boldsymbol{\mu}, \mathbf{K})). \quad (11)$$

Define the negative log probability for the posterior as $\psi(X) \triangleq -\log \tilde{q}^*(X)$. The Variational Inference objective is equivalent to

$$\mathcal{J}(q_\theta) = \text{KL}(q_\theta(\mathbf{X}) \parallel \tilde{q}^*(\mathbf{X})) = \mathbb{E}[\psi(X)] - \mathcal{H}(q_\theta),$$

where $\mathcal{H}(q_\theta)$ denotes the entropy of the distribution q_θ , which promotes the robustness of the motion plan solution. We add an additional temperature parameter, \hat{T} , to trade off this robustness, leading to the objective of temperature [14]

$$\mathcal{J}(q_\theta) = \text{KL}(q_\theta(\mathbf{X}) \parallel \tilde{q}^*(\mathbf{X})) = \mathbb{E}[\psi(X)] - \hat{T}\mathcal{H}(q_\theta) \quad (12)$$

3. KL-Proximal GVI Algorithm For Linear-Gaussian Systems

In this section, we derive a proximal point Gaussian Variational Inference algorithm for the GVIMP problem for linear-Gaussian system formulation (11).

3.1. Proximal Point Gaussian Variational Inference

(a) *KL-proximal point Variational Inference.* The proximal point, or proximal minimization algorithm in the Euclidean space, is defined by solving the following optimization problem at each step

$$x_{k+1} = \arg \min_x \mathcal{J}(x) + \frac{1}{2\beta_k} \|x - x_k\|_2^2, \quad (13)$$

where \mathcal{J} is the original objective in a minimization problem, $\|x - x_k\|_2^2$ is a quadratic regularizer centered around the previous iterate x_k , and β_k is the step size. The proximal point algorithm is shown to be more stable than vanilla gradient descent, as it can be interpreted as the backward Euler integration of the gradient flow [47, 48].

In the variational inference problems, the original objective is to maximize the ELBO, \mathcal{L} . The KL divergence is a better metric candidate than the Euclidean 2-norm for the regularizer. Replacing the 2-norm regularizer in (13) by the KL-divergence, we obtain at the KL-proximal point algorithm, which solves the following optimization at each step [49, 25]

$$\delta\theta_{k+1} = \arg \max_{\theta} \mathcal{L}(x, \theta) - \frac{1}{\beta_k} \text{KL}(q(x | \theta) \parallel q(x | \theta_k)). \quad (14)$$

(b) *Splitting in Variational Motion Planning.* To solve the proximal point iteration for general nonlinear ELBOs turned out to be challenging [26]. A commonly-encountered situation in variational inference is that the ELBO can be split into 2 parts, $-\mathcal{L} = \psi_e + \psi_d$, where the gradients of $\psi_e \triangleq \mathbb{E}_{q_\theta}[\log(f_e(x))]$ are easy to compute, sometimes are directly known in closed-form, e.g., for Gaussian priors and other conjugate models; and the computation of gradients of $\psi_d \triangleq \mathbb{E}_{q_\theta}[\log(f_d(x))]$ is not direct. In order to obtain the updates efficiently, first-order approximations can be performed on ψ_d , resulting in proximal gradient algorithms [47]. This decomposition is also known as ‘splitting’.

Inspired by this, we derive the splitting structure for the variational inference in the path distribution space for motion planning problems for the first time. We decompose the motion planning ELBO into two different parts

$$\begin{aligned} \mathcal{L}(x, \theta) &= \mathbb{E}_{q_\theta}[\log \tilde{\mathbb{Q}}^*] - \mathbb{E}_{q_\theta}[\log q_\theta] \\ &= -\mathbb{E}_{q_\theta} \left[\log q_\theta + \frac{1}{2} \|\mathbf{x} - \boldsymbol{\mu}\|_{\mathbf{K}^{-1}}^2 \right] - \mathbb{E}_{q_\theta}[V(\mathbf{x})], \end{aligned} \quad (15)$$

where we use the two functions ψ_e, ψ_d to denote the two parts

$$\psi_e(x, \theta) \triangleq \mathbb{E}_{q_\theta} \left[\log q_\theta + \frac{1}{2} \|\mathbf{x} - \boldsymbol{\mu}\|_{\mathbf{K}^{-1}}^2 \right], \quad (16a)$$

$$\psi_d(x, \theta) \triangleq \mathbb{E}_{q_\theta}[V(\mathbf{x})]. \quad (16b)$$

The function ψ_e is the negative likelihood of the prior cost-related term and the entropy, which is a conjugate model. The term ψ_d is the cost related to collision avoidance, which is non-conjugate. Consider the Gaussian distribution $q_e \sim \mathcal{N}(\boldsymbol{\mu}, \mathbf{K})$, then ψ_e can be written as the KL-divergence between q_θ and q_e up to a constant as

$$\psi_e(x, \theta) \propto \mathbb{E}_{q_\theta} (\log q_\theta - \log q_e) = \text{KL}(q_\theta \parallel q_e),$$

which indicates that the gradients of ψ_e with respect to $(\mu_\theta, \Sigma_\theta^{-1})$ have closed-form. For the non-conjugate model, ψ_d , we approximate this term ψ_d to the first order. The splitting and first-order approximation lead to the following KL proximal gradient update at each iteration.

(c) *The KL-proximal gradients with splitting.* After splitting, we derive the update step of the KL-proximal algorithm. Substituting the terms ψ_e and ψ_d in (16) into (14), we have

$$\theta_{k+1} = \underset{\theta}{\operatorname{argmin}} \mathcal{J}_{\text{ProxKL}} \quad (17)$$

$$\triangleq \underset{\theta}{\operatorname{argmin}} \theta^T [\nabla \psi_d(\theta_k)] + \psi_e(\theta) + \frac{\text{KL}(q_\theta(\mathbf{x}) \parallel q(\mathbf{x} | \theta_k))}{\beta_k}.$$

Taking the first-order gradients with respect to $(\mu_\theta, \Sigma_\theta^{-1})$, we obtain the KL-proximal updates for them. The update rule is summarized in the following Theorem 1, whose proof can be found in Appendix A.

Theorem 1. *The KL-proximal updates for $(\mu_\theta, \Sigma_\theta^{-1})$ are*

$$(\mathbf{K}^{-1} + \frac{\Sigma_\theta^{-1}}{\beta_k}) \mu_{\theta_{k+1}} = -\nabla_{\mu_\theta} \psi_d + \mathbf{K}^{-1} \boldsymbol{\mu} + \frac{\Sigma_\theta^{-1}}{\beta_k} \mu_{\theta_k}, \quad (18a)$$

$$\Sigma_{\theta_{k+1}}^{-1} = \frac{\beta_k}{\beta_k + 1} (2\nabla_{\Sigma_\theta} \psi_d + \mathbf{K}^{-1} + \frac{\Sigma_\theta^{-1}}{\beta_k}). \quad (18b)$$

Remark. *We remark that this update rule is accurate in the sense that we directly approximate the expected term $\psi_d(\theta) = \mathbb{E}_{q(\mathbf{x}|\theta)} [\|\mathbf{h}(\mathbf{x})\|_{\Sigma_{\text{obs}}}^2]$ to the first-order, instead of approximating the integrand inside the expectation.*

(d) *Connection to Natural Gradient Descent (NGD).* The NGD [24, 15] updates can be integrated into the proximal point algorithms with a symmetric KL-divergence being the proximal regularizer [13]. Specifically, the natural gradient descent update step with unit step size is

$$\delta\theta = G(\theta)^{-1} \nabla_\theta \mathcal{L}(x, \theta),$$

where $G(\theta) \triangleq \mathbb{E}_{q_\theta} [\nabla_\theta \log q_\theta (\nabla_\theta \log q_\theta)^T]$ is the Fisher information matrix. It is the solution to the following proximal point algorithm with the first-order approximation of the ELBO

$$\delta\theta = \underset{d\theta}{\operatorname{argmin}} d\theta^T \nabla_\theta \mathcal{L}(x, \theta) + d\theta^T G(\theta) d\theta \quad (19)$$

$$\approx \underset{d\theta}{\operatorname{argmin}} d\theta^T \nabla_\theta \mathcal{L}(x, \theta) + \text{KL}^{\text{sym}}(q(x | \theta) \parallel q(x | \theta + d\theta)),$$

where the symmetric KL divergence KL^{sym} between 2 distributions q_1 and q_2 is defined as

$$\text{KL}^{\text{sym}}(q_1 \parallel q_2) \triangleq \text{KL}(q_1 \parallel q_2) + \text{KL}(q_2 \parallel q_1).$$

With a step size β_k , the NGD update is equivalent to changing the proximal operator in (17) from the KL divergence to the symmetric KL divergence.

4. Sparse Factor Graph For Marginal Computation

In the KL-proximal updates (18), computing the gradients $\nabla_{\mu_\theta} \psi_d$ and $\nabla_{\Sigma_\theta} \psi_d$ represents the computational bottleneck. This section introduces a paradigm that leverages the underlying sparse motion planning factor graph to distribute this computation onto the marginal levels.

4.1. Sparse Motion Planning Factor Graph

For clarity, denote $\psi(\mathbf{x}) = V(\mathbf{x})$ in (16b). With some algebraic calculation, the gradients of ψ_d are given by

$$\nabla_{\mu_\theta} \psi_d(\theta) = \Sigma_\theta^{-1} \mathbb{E} [(\mathbf{x} - \mu_\theta) \psi] \quad (20a)$$

$$\nabla_{\Sigma_\theta} \psi_d(\theta) = -\frac{1}{2} \Sigma_\theta^{-1} \mathbb{E} [\psi] + \frac{1}{2} \Sigma_\theta^{-1} \mathbb{E} [(\mathbf{x} - \mu_\theta)(\mathbf{x} - \mu_\theta)^T \psi] \Sigma_\theta^{-1}, \quad (20b)$$

which can be broken apart into the calculation of the expectations of ψ

$$\mathbb{E} [\psi], \quad \mathbb{E} [(\mathbf{x} - \mu_\theta) \psi], \quad \mathbb{E} [(\mathbf{x} - \mu_\theta)(\mathbf{x} - \mu_\theta)^T \psi].$$

The motion planning factor graph is shown in the following Fig. 1. It contains two types of factors, the $f_{i,i+1}(x_i, x_{i+1})$ represents the prior factor enforcing the kinodynamics constraints, and the $f_i(x_i)$ are the collision factors that encourage the trajectory remain within obstacle-free regions.

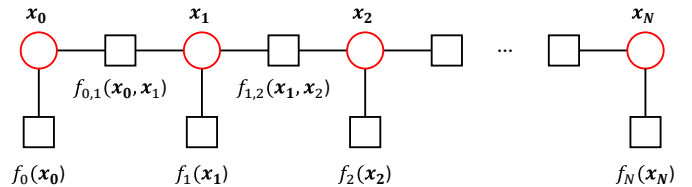


Figure 1: The GVIMP factor graph.

This factorized structure can be leveraged to distribute the computation of ψ_d on a GPU. Given the factor graph structure, the collision costs $\psi_d = \|\mathbf{h}(x)\|_{\Sigma_{\text{obs}}}^2$ can be factorized into

$$\psi_d = \psi_0^d(q_0), \dots, \psi_N^d(q_N),$$

where the factorized potentials are defined as the collision cost on each individual state on the trajectory

$$\psi_i^d \triangleq \|\mathbf{h}_i(q_i)\|_{\Sigma_{\text{obs}}}^2.$$

The factor-level marginal Gaussian variables are linearly mapped from the joint Gaussian

$$q_i \sim \mathcal{N}(\mu_\theta^i, \Sigma_\theta^i), \quad \mu_\theta^i = M_i \mu_\theta, \quad \Sigma_\theta^i = M_i \Sigma_\theta M_i^T. \quad (23)$$

Nest, we explore these sparsity patterns in the proposed Gaussian distributions.

4.2. Marginal updates

By Stein's Lemma, we write (20a) and (20b) as

$$\nabla_{\mu_\theta} \psi_d(\mathbf{x}, \theta) = \mathbb{E} [\nabla_{\mathbf{x}} \psi(\mathbf{x})], \quad (24a)$$

$$\nabla_{\Sigma_\theta} \psi_d(\mathbf{x}, \theta) = \frac{1}{2} \mathbb{E} [\nabla_{\mathbf{xx}}^2 \psi(\mathbf{x})]. \quad (24b)$$

Since we can decompose the $\psi(\mathbf{x})$ to marginal level

$$\psi(\mathbf{x}) = \sum_{n=1}^{N-1} \psi_i(\mathbf{x}_i) = \sum_{i=1}^{N-1} \|\mathbf{h}(\mathbf{x}_i)\|_{\Sigma_{\text{obs}_i}}^2, \quad (25)$$

where $\mathbf{x}_i = M_i \mathbf{x}$ is a subset of the variables relevant to the i th factor as defined in (23). Applying the factorization (25) to (24a), we obtain

$$\mathbb{E}_q [\nabla_{\mathbf{x}} \psi(\mathbf{x})] = \sum_{i=1}^{N-1} M_i^T E_{q_i} [\nabla_{\mathbf{x}_i} \psi_i(\mathbf{x}_i)]. \quad (26)$$

For the i -th factor, we can simplify the gradient and expectation to being over just \mathbf{x}_i , since ψ_i only depends on \mathbf{x}_i . We have a similar result for (24b)

$$\mathbb{E}_q [\nabla_{\mathbf{xx}}^2 \psi(\mathbf{x})] = \sum_{i=1}^{N-1} M_i^T \mathbb{E}_{q_i} [\nabla_{\mathbf{x}_i \mathbf{x}_i}^2 \psi_i(\mathbf{x}_i)] M_i \quad (27)$$

Apply Stein's Lemma again to (26) and (27), we have

$$\nabla_{\mu_\theta} \psi_d(\mathbf{x}, \theta) = \sum_{i=1}^{N-1} M_i^T \nabla_{\mu_\theta} \psi_i^d(\mathbf{x}_i, \theta_i), \quad (28a)$$

$$\nabla_{\Sigma_\theta} \psi_d(\mathbf{x}, \theta) = \sum_{i=1}^{N-1} M_i^T \nabla_{\Sigma_\theta} \psi_i^d(\mathbf{x}_i, \theta_i) M_i. \quad (28b)$$

The factorization of ψ_d allows us to decompose the computation of its gradients across marginal distributions. Combined with parallel processing on a GPU, this structure significantly improves the computational efficiency of the algorithm.

4.3. Sparse Quadratures for Expectation Estimations

Our primary goal is to estimate the expectation (28) on the marginal levels. Gauss-Hermite quadrature approximations are widely used in filtering literatures [50, 32], as well as motion planning [14, 15]. Cubature approximations are accurate and efficient for lower dimensional problems. However, for higher dimensional problems, a straight-forward tensor product of the full-grid sigma points scale exponentially with the dimension, making it infeasible for high-dimensional problems [51].

Sparse-grid quadrature rules (Smoyak's rules) [52, 53] ignore the cross terms among different dimensions to mitigate the curse of dimensionality, resulting in a quadrature rule with polynomial dimensional dependence. In this work, we adopt the sparse-grid Gauss-Hermite quadrature rules to estimate (28). To integrate a scalar function $\varphi(\mathbf{x})$

$$\int \varphi(\mathbf{x}) \mathcal{N}(\mathbf{x}; m, P) d\mathbf{x},$$

G-H quadrature methods consist of the following steps

1. Compute the p roots of a p th order Hermite polynomial, also denoted as *sigma points*: $\xi = [\xi_1, \dots, \xi_p]$.
2. Compute the *weights*: $W_i = \frac{p!}{p^2 [H_{p-1}(\xi_i)]^2}, i = 1, \dots, p$.
3. Approximate:

$$\int \varphi(\mathbf{x}) \mathcal{N}(\mathbf{x}; m, P) d\mathbf{x} \approx \sum_i W_i \varphi(\sqrt{P} \xi_i + m). \quad (29)$$

Lemma 1 (Smoyak sparse quadrature complexity). *For a n -variate function, the number of computations needed by a sparse grid quadrature that is exact for $p = 2k_q - 1$ total polynomial order is bounded by [53]*

$$\frac{e^{k_q}}{(k_q - 1)!} n^{k_q}$$

which has a polynomial dependence on the desired precision.

Algorithm 1: PGVIMP (LTV system).

input : LTV system $\{(A_t, a_t, B_t)\}_{t=1}^N$; Number of factors L ; Upper bound of KL divergence ϵ

output: Optimized trajectory distribution $\mathcal{N}(\mu_\theta^*, \Sigma_\theta^*)$.

- 1 For $i = 0, \dots, N$, compute the state transitional kernel $\Phi_{i,i+1}$, the Grammian $Q_{i,i+1}$, and the prior mean trajectory μ_i .
 - 2 Compute prior precision \mathbf{K}^{-1} and prior mean μ
 - 3 **for** $k = 1, 2, \dots$ **do**
 - 4 Compute marginals using GBP (23), (36).
 $\{q_\ell \sim \mathcal{N}(\mu_\theta^\ell, \Sigma_\theta^\ell)\}_{\ell=1}^L \leftarrow (\mu_\theta, \Sigma_\theta^{-1})$
 - 5 Parallel Computing the collision factors.
 - 6 Mapping the gradients back to the joint level
 $(\nabla_{\mu_\theta} \psi_d(\mathbf{x}), \nabla_{\Sigma_\theta} \psi_d(\mathbf{x})) \leftarrow$
 $\{(\nabla_{\mu_\theta^\ell} \psi_\ell^d(\mathbf{x}_\ell), \nabla_{\Sigma_\theta^\ell} \psi_\ell^d(\mathbf{x}_\ell), M_\ell)\}_\ell$
 - 7 Select the largest β_k using bisection such that:
 $\text{KL}(q_{\theta_{k+1}} \| q_{\theta_k}) \leq \epsilon, \quad \Sigma_{\theta_k}^{-1} > 0$
 - 8 Compute $\mu_{\theta_{k+1}}$ and $\Sigma_{\theta_{k+1}}^{-1}$ using (18)
 $(\mu_{\theta_{k+1}}, \Sigma_{\theta_{k+1}}^{-1}) \leftarrow (\mu_{\theta_k}, \Sigma_{\theta_k}^{-1}, \nabla_{\mu_\theta} \psi_d, \nabla_{\Sigma_\theta} \psi_d, \mathbf{K}^{-1}, \mu)$
-

Algorithm 2: i-PGVIMP (Nonlinear system).

input : Nonlinear system $\{(f_t, g_t)\}_{t=1}^N$, stepsize η ; Nominal trajectory $\{(\bar{x}_t^0, \bar{\Sigma}_t^0)\}$.

output: Optimized trajectory distribution $\mathcal{N}(\mu_\theta^*, \Sigma_\theta^*)$.

- 1 **for** $i = 0, \dots, N$ **do**
 - 2 Linearize the nonlinear system using SLR
 $\{(A_t^i, a_t^i, B_t^i)\} \leftarrow \text{SLR}(f_t, g_t, \bar{x}_t^i, \bar{\Sigma}_t^i)$
 - 3 Perform P-GVIMP (Algorithm 1) on the linearized system
 - 4 $\{(\bar{x}_t^{i+1}, \bar{\Sigma}_t^{i+1})\} \leftarrow \text{P-GVIMP}(A_t^i, a_t^i, B_t^i)$
-

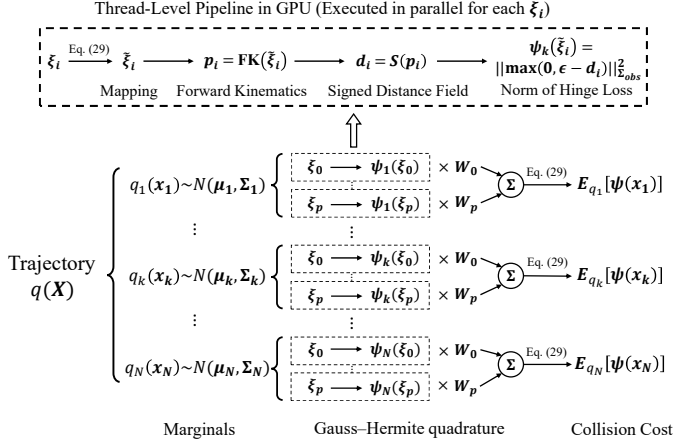


Figure 2: Parallel collision checking

$L = 2N + 3$ factors, the maximum dimension being $d = 2n$. A serial computation of the nonlinear factors leads to a linear dependence on N , and the total complexity is $O(N \times n^{k_q})$, where k_q is the desired precision in the GH-quadrature [15]. Experimentally, to obtain a precise estimate of the collision costs, $k_q \geq 6$ is required. The parallel nonlinear factor computation is of complexity $O(n)$, and the complexity of computing the marginal covariances for the tree-structured factor graph using GBP is of $O(N \times n^3)$. The overall complexity of the algorithm is therefore reduced from $O(N \times n^{k_q})$ to $O(N \times n^3)$, which is not dependent on the quadrature precision k_q .

6. Iterative P-GVIMP for Nonlinear Systems

Many robot dynamical systems are nonlinear. The P-GVIMP algorithm described in the previous sections constrained the system to be LTV. To handle the nonlinearity, this section introduces our proposed Iterative Parallel GVIMP Algorithm (i-PGVIMP).

6.1. Gaussian Assumptions for Nonlinear Transition

It is in general difficult to solve the FPK for arbitrary nonlinear stochastic system (1). Gaussian assumption is popular in the robotics applications, especially in the filtering and estimation [32, 31]. It assumes the state distribution follows

$$\frac{d\bar{X}_t}{dt} = \mathbb{E}_{\mathcal{N}} [f(X_t)], \quad (37a)$$

$$\begin{aligned} \frac{d\text{Cov}(X_t)}{dt} &= \mathbb{E}_{\mathcal{N}} [f(X_t)(X_t - \bar{X}_t)^T] + \mathbb{E}_{\mathcal{N}} [(X_t - \bar{X}_t)f(X_t)^T] \\ &+ \mathbb{E}_{\mathcal{N}} [g_t(X_t)g_t(X_t)^T], \end{aligned} \quad (37b)$$

where $\mathbb{E}_{\mathcal{N}} [\psi(\cdot)] \triangleq \int \psi(x)\mathcal{N}(x)$ denotes the expected values under Gaussian distributions.

We adopt the Gaussian assumptions (37) and propose an iterative statistical linearization of the nonlinear system around a nominal trajectory. In this way, each iteration produces a LTV system from the linearization. We then perform the P-GVIMP algorithm 1 on the obtained linearized LTV system. The results are used in the next iteration for the SLR linearization. This process is performed until the linearization loop converges.

6.2. Iterative Statistical Linear Regression (SLR)

Statistical linear regression (SLR) [50] is a statistical method to approximate the nonlinear stochastic processes locally. The linearization results in an LTV system depending on the state at which the linearization is performed.

Assuming the closed-loop discrete nonlinear stochastic dynamics at time $t = t_i$ as $X_{i+1} = f_{cl}(X_i)$, then the goal of SLR is to find a linear model (A_i, a_i)

$$\hat{X}_{i+1} = A_i X_i + a_i$$

to minimize the statistical error, i.e.,

$$\{A_i, a_i\} = \arg \min \mathbb{E} [\|X_{i+1} - \hat{X}_{i+1}\|^2]. \quad (38)$$

Taking the first-order derivative with respect to a_i and let it be zero, we arrive at

$$a_i^* = \mathbb{E} [f_{cl}(X_i)] - A_i^* \mathbb{E} [X_i]. \quad (39)$$

substituting (39) into (38), the gradients over A_i is

$$(f_{cl}(X_i) - \mathbb{E} [f_{cl}(X_i)] - A_i (X_i - \mathbb{E} [X_i])) (X_i - \mathbb{E} [X_i])^T,$$

letting which be zero leads to

$$A_i^* = P_{yx} P_{xx}^{-1}, \quad (40)$$

where P_{yx}, P_{xx} are defined respectively as

$$P_{yx} \triangleq (f_{cl}(X_i) - \mathbb{E} [f_{cl}(X_i)])(X_i - \mathbb{E} [X_i])^T \quad (41)$$

$$P_{xx} \triangleq (X_i - \mathbb{E} [X_i])(X_i - \mathbb{E} [X_i])^T. \quad (42)$$

From (39) and (40), the computation of (a_i^*, A_i^*) involves the computation of the expectations of a nonlinear function $\mathbb{E} [f_{cl}(X_i)]$, which in this paper we use the sparse GH-quadrature rules mentioned in Lemma 1. Specifically, at time t_i , for a given desired approximation precision, k_q , we compute the set of weights and sigma points $\{(W_l^i, \xi_l^i)\}_{l=1}^{k_q}$ for the sparse quadrature, and perform the quadrature approximation

$$\mathbb{E} [X_{i+1}] = \mathbb{E} [f_{cl}(X_i)] \approx \sum_{l=1}^{k_q} W_l^i f(\sqrt{P_{xx}} \xi_l^i + \mathbb{E} [X_i]),$$

which is then substituted into (39) and (40). This procedure is iteratively performed forward in time. The iterative Parallel GVIMP is summarized in Algorithm 2.

7. experiments

This section presents the numerical experiment results for the proposed method. The experiments are aimed to answer the following questions:

- **Q1:** How much efficiency do we gain by leveraging the parallel computations on GPUs, compared with serial computations on CPUs?

- **Q2:** The effectiveness of the KL-proximal algorithm in high-DOF robot motion planning tasks, and its comparison with the GPMP2 baseline;
- **Q3:** The effectiveness of the iterative PGVIMP algorithm in motion planning tasks for nonlinear dynamical systems.

To answer these questions, we first demonstrate the efficiency improvement brought by the parallel computing paradigm on a laptop GPU. Secondly, we show the planning results for two 7-DOF linear robotics kinematic problems. Thirdly, we show the planning results for a linearized system and a full nonlinear planar quadrotor system. Finally, we present some ablation study results and comparisons with baseline methods.

7.1. Efficiency Improvement through Parallel Computation

The first set of experiments is conducted to showcase the improved computation efficiency by leveraging the parallel computations on a GPU. Efficiency improvement is gained from parallel collision cost computation and the computing of marginal covariances using GBP.

(a) *Parallel collision-checking on a dense trajectory.* To demonstrate the improvement in collision-checking efficiency on a dense trajectory, we first compare the time of computing the expected collision factors between the proposed GPU parallel computation and a serial implementation [15]. We made the comparison on 2D / 3D point robots and 7-DOF WAM arm robots with linear time-invariant (LTI) system

$$A_t = \begin{bmatrix} 0 & I \\ 0 & 0 \end{bmatrix}, a_t = \begin{bmatrix} 0 \\ 0 \end{bmatrix}, B_t = \begin{bmatrix} 0 \\ I \end{bmatrix}. \quad (43)$$

	2D Point Robot	3D Point Robot	7-DoF WAM
Serial	85.40 ms	479.7 ms	8010.5 ms
Parallel	14.80 ms	37.60 ms	306.16 ms
Improvement	82.67 %	92.16 %	96.18 %

Table 1: Implementation time comparison for Cost Expectation Estimations (quadrature precision degree: $k_q = 10$ for 2D and 3D Point Robots, and $k_q = 6$ for 7-DoF WAM Arm; time discretization $N = 750$).

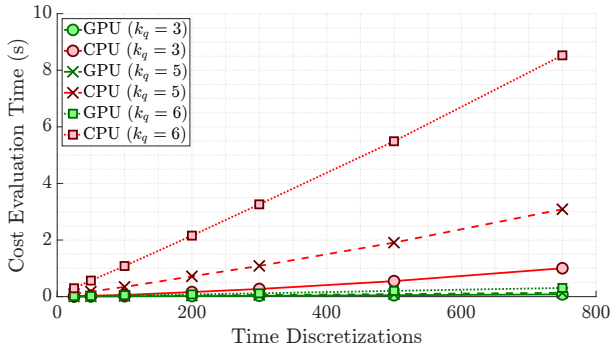


Figure 3: 7-DOF WAM expected collision cost computation.

The results are shown in Tab. 1. On a dense trajectory (time discretization $N = 750$), we achieved over 95% improvement in the computation time compared with serial implementation

on a CPU. Fig. 3 shows the computation time spent on the expected collision checking cost computation for different time discretizations. We observe that the parallel implementation is insensitive to the time discretization.

(b) *GBP for computing the marginal covariances.* Next, we demonstrate the efficiency improvement in computing the marginal covariances achieved through GBP. We compare with the brute-force way of computing the inverse of the precision matrix, Σ_θ^{-1} , using a direct matrix inversion. The comparison results are in Tab. 2 and Fig. 4. We see a linear dependence on the number of time discretizations for GBP, and a polynomial (N^3) dependence of direct inversion. A 99.5% improvement in implementation time is gained through GBP for a 7-DOF WAM.

	2D Point Robot	3D Point Robot	7-DoF WAM
Brute force	256.4 ms	456.86 ms	1234.04 ms
GBP	2.36 ms	3.01 ms	6.04 ms
Improvement	99.07 %	99.34 %	99.51 %

Table 2: Implementation Time Comparison for Precision Matrix Inversion (Dimension of Precision: 5000, 4998, 4998).

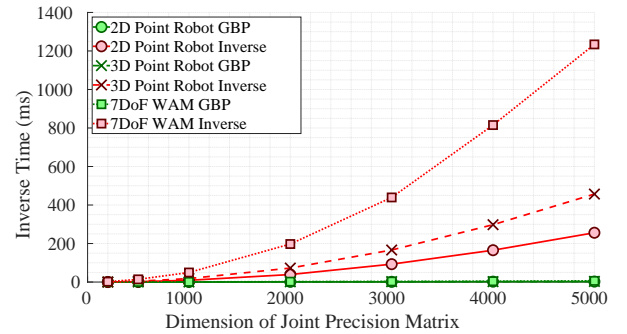


Figure 4: Time-Dimension curve for precision matrix inversion.

(c) *The overall optimization time.* Finally, we show the overall efficiency of the proposed paradigm by recording the total optimization time, and comparing with CPU serial implementation [14, 15]. The results are recorded in Tab. 3. We gained over 97% improvement for the 7-DOF planning problems.

	2D Point Robot	3D Point Robot	7-DoF WAM
Serial	7.38 s	27.07 s	425.03 s
Parallel	0.48 s	1.12 s	12.25 s
Improvement	93.50 %	95.86 %	97.11 %

Table 3: Implementation Time Comparison for the whole optimization process (quadrature precision degree: $k_q = 10$ for 2D and 3D Point Robots, and $k_q = 6$ for 7-DoF WAM Arm; time discretization $N = 750$).

7.2. Planning Results for the 7-DOF Robot Arms

Next, we show the motion planning result for 2 models of 7-DOF robot arms, the WAM robot Arm [54], and the right arm of the PR2 robot [55]. We then visualize the results in the Robot Operating System (ROS) [56] with a high-fidelity robot model for both models integrated into the *Moveit* [57] motion

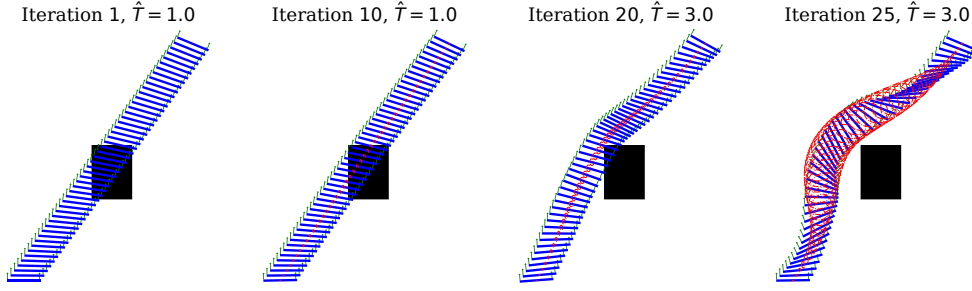


Figure 5: Convergence of P-GVIMP inner-loop iterations for the linearized planar quadrotor system.

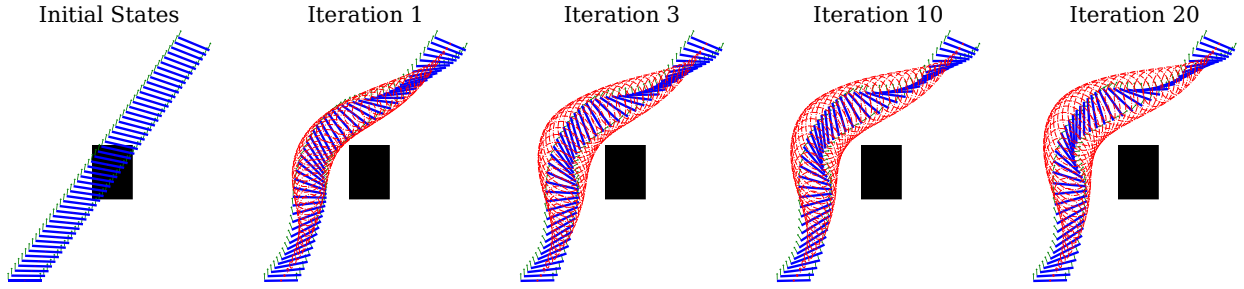


Figure 6: Convergence of the SLR iterations for the nonlinear planar quadrotor dynamical system.

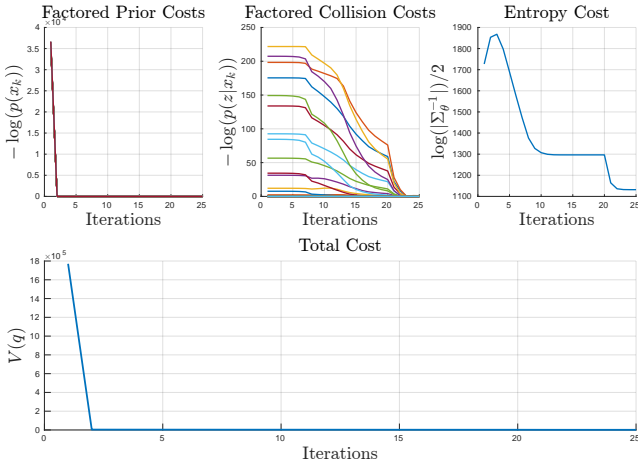


Figure 7: Factorized and total costs in Fig. 5.

planning package. Fig. 8 shows the planning results for the WAM robot arm, and Fig. 9 shows the results for the PR2 robot arm planning results. The experiment settings are listed in Tab. C.7

7.3. Iterative PGVIMP for nonlinear dynamical system

We validate our proposed algorithm on a planar quadrotor system defined as

$$\dot{X}_t = \begin{bmatrix} v_x \cos(\phi) - v_z \sin(\phi) \\ v_x \sin(\phi) + v_z \cos(\phi) \\ \dot{\phi} \\ v_z \dot{\phi} - g \sin(\phi) \\ -v_x \dot{\phi} - g \cos(\phi) \\ 0 \end{bmatrix} + \begin{bmatrix} 0 & 0 \\ 0 & 0 \\ 0 & 0 \\ 0 & 0 \\ 1/m & 1/m \\ l/J_q & -l/J_q \end{bmatrix} \begin{bmatrix} u_1 \\ u_2 \end{bmatrix}, \quad (44)$$

Iteration	1	3	10	20
Norm difference	286.40	16.61	4.33	2.96

Table 4: Norm of trajectory difference between two consecutive linearizations of the nonlinear dynamics.

where g is the gravity, m represents the mass of the planar quadrotor, l is the length of the body, and J_q is the moment of inertia. u_1 and u_2 are the two thrust inputs to the system. In all our experiments, we set $m = 1/\sqrt{2}$, $l = \sqrt{2}$, and $J_q = 1$. We linearize the system (44) around an initial nominal mean trajectory and perform the P-GVIMP algorithm on the obtained LTV system.

(a) *Convergence for LTV system.* We first show the results for a **linearized** planar quadrotor system, using Algorithm 1. We show the convergence of the algorithm via a downsampled plot of the intermediate proposal Gaussian trajectory distributions in Fig. 5 with the low and high temperatures \hat{T} in (12), and the corresponding cost evolutions, both for prior and collision factorized costs, and the total cost, in Fig. 7. After obtaining a collision-free trajectory with low temperatures, we switched to a high-temperature phase to put more weight on the entropy costs. The total costs keep decreasing throughout both processes.

(b) *Planning results for the nonlinear planar quadrotor.* Next, we consider the **full** nonlinear planar quadrotor system (44) using the iterative-PGVIMP planning, i.e., Algorithm 2. We compute the norm of the trajectory difference between consecutive iterations, and the iterations are stopped once the norm difference is below a threshold. The results are recorded in Tab. 4, and the planning results are shown in Fig. 6.

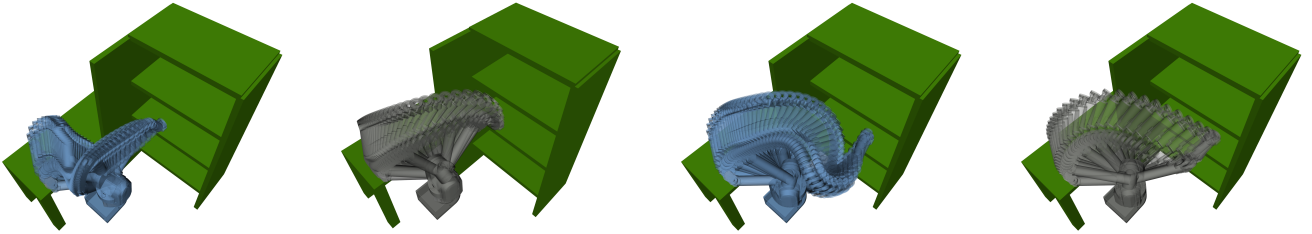


Figure 8: Planning results for the WAM Robot for two tasks with $N = 750$ states. The results are obtained from two algorithms: GPMP2 (blue) and KL-Proximal (Gray). For KL-Proximal, the settings are $T = 2.0$ and 2.75 , $\Sigma_{obs} = 20I$ and $19I$, The ratio between temperatures are $\hat{T}_{high}/\hat{T}_{low} = 10$ and 15 , respectively, and $r + \epsilon_{sdf} = 0.21$

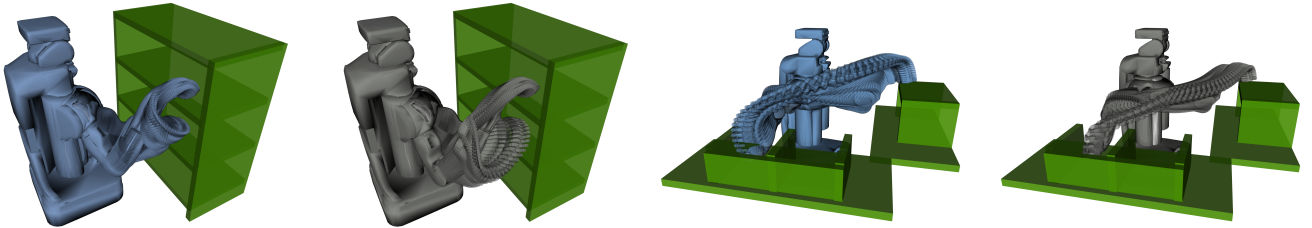


Figure 9: Planning results for the PR2 Robot for two tasks with $N = 750$ states. The results are obtained from two algorithms: GPMP2 (blue) and KL-Proximal (Gray). For KL-Proximal, the settings are $T = 2.25$ and 2.0 , $\Sigma_{obs} = 7.5I$ and $5I$, respectively, the ratio between temperatures is $\hat{T}_{high}/\hat{T}_{low} = 10$, and $r + \epsilon_{sdf} = 0.21$

	WAMExp 1	WAMExp 2	PR2Exp 1	PR2Exp 2
P-GVIMP	10.26s	9.48s	14.03s	11.86s
GPMP2	0.75s	1.36s	2.74s	0.78s

Table 5: The optimization time comparison for P-GVIMP and GPMP2 algorithms in the 7-DOF WAM and PR2 experiments with $n = 750$ support states, averaged over 50 runs. For a 7-DOF robot, the GPMP2 algorithm has $14 \times 750 = 10,500$ optimization variables, while the KL-Proximal GVI has $14 \times 750 + (3 \times 750 - 2) \times (14 \times 14) = 443,608$ optimization variables.

(c) *More experiments with different settings.* We did experiments for 4 different settings. We have 1 obstacle in the environment. The start and goal states in the 4 experiments are specified in the following Tab. C.8.

Fig. 11 shows the results of the nonlinear system of the planar quadrotor (44) for the 4 experiment settings.

(d) *Go through or go around a narrow gap? Robust motion planning through entropy regularization.* As motion planning with obstacles is a naturally non-convex problem, the solution is multi-modal. In the decision-making for motion planning, the risk and robustness of the solution are taken into consideration in our formulation by introducing the entropy of q_θ into the objective. This section shows an experiment for the planar quadrotor to fly through a narrow gap [14]. Two motion plans are obtained for the same motion planning task, as shown in Fig. 10. One plan (go-through plan) is visually riskier than the other (go-around plan). Our formulation provides a computable metric to compare the total cost consisting of optimality and robustness, between the two plans. In Tab. 6, we compute the sum of the prior and the collision costs, the entropy costs, and the total costs. By introducing lower entropy costs, our method selects the plan with lower risk over a shorter but riskier plan.

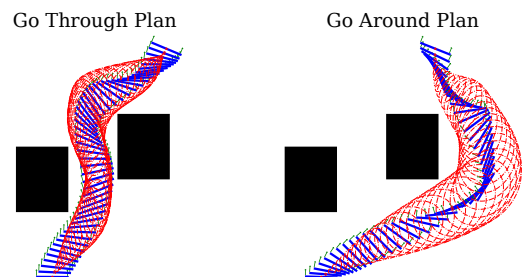


Figure 10: Entropy regularized robust planning in a narrow gap environment.

	Prior	Collision	MP	Entropy	Total
Go Through	138.96	1.26	140.22	1232.36	1372.58
Go Around	149.34	0.0369	149.38	1163.22	1312.6

Table 6: Comparing costs for two plans in Fig. 10. The ‘MP’ is short for the sum of prior and collision costs, representing the optimality, and entropy represents the robustness.

8. conclusion

In this work, we propose a distributed Gaussian Variational Inference approach to solve motion planning under uncertainties. The optimal trajectory distribution to a stochastic control problem serves as the target posterior in a variational inference paradigm. We leveraged this inference’s underlying sparse factor graph structure and proposed a distributed computation framework to solve the VI problem in parallel on GPU. Numerical experiments show the effectiveness of the proposed methods on an LTV system, and comparison studies demonstrated the computational efficiency.

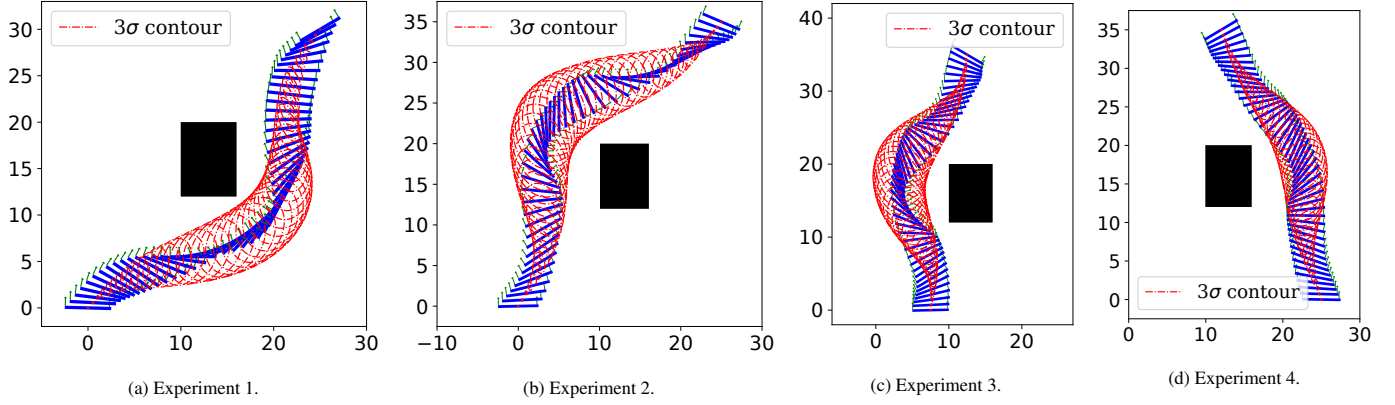


Figure 11: Results of the i-PGVIMP for the nonlinear planar quadrotor dynamical system. $N = 50$ support states are used, time span $T = 4.0 \sim 6.0$, radius $r + \epsilon_{sdf} = 1.5$, $\Sigma_{obs} = 6.0I \sim 7.5I$, low temperature $\hat{T}_{low} = 1.0$, high temperature $\hat{T}_{high} = 5.0$.

Appendix A. Proof of Theorem 1

Proof. First take the gradient of the objectives in (17) with respect to μ_θ and let it to be zero, we have

$$0 = \nabla_{\mu_\theta} \psi_d(\theta_k) + \mathbf{K}^{-1}(\mu_\theta - \boldsymbol{\mu}) + \frac{1}{\beta_k} \Sigma_{\theta_k}^{-1}(\mu_\theta - \mu_{\theta_k}),$$

from which we have the update for the mean as

$$(\mathbf{K}^{-1} + \frac{1}{\beta_k} \Sigma_{\theta_k}^{-1}) \mu_{\theta_{k+1}} = -\nabla_{\mu_\theta} \psi_d(\theta_k) + \mathbf{K}^{-1} \boldsymbol{\mu} + \frac{1}{\beta_k} \Sigma_{\theta_k}^{-1} \mu_{\theta_k}.$$

Since $\nabla_{\Sigma_\theta^{-1}}(\cdot) = -\Sigma_\theta \nabla_{\Sigma_\theta}(\cdot) \Sigma_\theta$, the necessary condition for the update rule for Σ_θ^{-1} can be derived by taking the gradients of the objectives in (17) with respect to Σ_θ and letting it to be zero, leading to

$$0 = \nabla_{\Sigma_\theta} \psi_d(\theta_k) + \frac{1}{2} \left(\frac{1}{\beta_k} \Sigma_{\theta_k}^{-1} + \mathbf{K}^{-1} - (1 + \frac{1}{\beta_k}) \Sigma_{\theta_{k+1}}^{-1} \right),$$

from which we obtain the update rule for the Σ_θ^{-1} as

$$\Sigma_{\theta_{k+1}}^{-1} = \frac{\beta_k}{\beta_k + 1} \left(2 \nabla_{\Sigma_\theta} \psi_d(\theta_k) + \mathbf{K}^{-1} + \frac{1}{\beta_k} \Sigma_{\theta_k}^{-1} \right).$$

□

Appendix B. PGVIMP Algorithm Implementation Details

We present implementation details of the PGVIMP Algorithm 1.

(a) *Step size selection.* The proximal point algorithm is one type of gradient descent algorithm, which does not guarantee that the updated distribution at each step remains inside the distribution family \mathcal{Q} , especially with the step sizes being too large. For instance, the covariance updates in the Gaussian case does not guarantee that the updated covariances are always positive definite. We control the step size β_k to enhance convergence efficiency by setting an upper bound on the KL divergence between the updated and current distributions. By solving the

convex optimization problem

$$\begin{aligned} \beta_k^* &= \max_{\beta_k > 0} \beta_k \\ \text{s.t. } & \text{KL}(q_{\theta_{k+1}}(\mathbf{x}) \| q_{\theta_k}(\mathbf{x})) \leq \epsilon, \Sigma_{\theta_{k+1}}^{-1} > 0, \end{aligned} \quad (\text{B.1})$$

we are able to find the largest step size β_k that satisfies the constraints, ensuring both stability and efficient convergence. In practice, we use a bi-section algorithm to choose a suitable stepsize that keeps the next step distribution close to the current one.

Appendix C. Experiment Settings

We record the settings for different experiments we conducted in this work in Tab. C.7 and Tab. C.8.

	Start & Goal
WAMExp 1	[-0.8, -1.70, 1.64, 1.29, 1.1, -0.106, 2.2] [0, 0.94, 0, 1.6, 0, -0.919, 1.55]
WAMExp 2	[-0.9, -1.7, 1.34, 1.19, 0.8, -0.126, 2.5] [-0.7, -1.35, 1.2, 1.0, -0.7, -0.1, 1.2]
PR2Exp 1	[-0.7, 0.175, -0.785, -1.05, -2.88, -0.6, 0.785] [-0.174, 0.785, -0.26, -0.785, 1.57, -0.35, 1.57]
PR2Exp 2	[-1.9, 0.15, -2.18, -0.524, 3.14, -0.524, -1.047] [0, 0.171, 0, -0.96, 3.14, -0.785, 0]

Table C.7: 7-DOF Robot Arm Planning Experiment Settings.

	Start	Goal
Exp 1	[0, 0, 0, 0, 0, 0]	[25, 30, $\pi/6$, -1, 2, 0.01]
Exp 2	[0, 0, 0, 0, 0, 0]	[25, 35, $-\pi/8$, 1, 2, 0.01]
Exp 3	[10, 0, 0, 0, 0, 0]	[5, 35, $-\pi/6$, 1, 2, -0.02]
Exp 4	[25, 0, 0, 0, 0, 0]	[12, 35, $\pi/6$, -2, 1, 0]

Table C.8: Planar Quadrotor Planning Experiment Settings.

References

- [1] S. M. LaValle, *Planning algorithms*, Cambridge university press, 2006.
- [2] D. González, J. Pérez, V. Milanés, F. Nashashibi, A review of motion planning techniques for automated vehicles, *IEEE Transactions on intelligent transportation systems* 17 (4) (2015) 1135–1145.
- [3] N. Ratliff, M. Zucker, J. A. Bagnell, S. Srinivasa, Chomp: Gradient optimization techniques for efficient motion planning, in: *IEEE international conference on robotics and automation*, 2009, pp. 489–494.
- [4] J. Schulman, Y. Duan, J. Ho, A. Lee, I. Awwal, H. Bradlow, J. Pan, S. Patil, K. Goldberg, P. Abbeel, Motion planning with sequential convex optimization and convex collision checking, *The International Journal of Robotics Research* 33 (9) (2014) 1251–1270.
- [5] G. Chen, H. Yu, W. Dong, X. Sheng, X. Zhu, H. Ding, What should be the input: Investigating the environment representations in sim-to-real transfer for navigation tasks, *Robotics and Autonomous Systems* 153 (2022) 104081.
- [6] W.-H. Chen, D. J. Ballance, P. J. Gawthrop, J. O’Reilly, A nonlinear disturbance observer for robotic manipulators, *IEEE Transactions on industrial Electronics* 47 (4) (2000) 932–938.
- [7] M. Kalakrishnan, S. Chitta, E. Theodorou, P. Pastor, S. Schaal, Stomp: Stochastic trajectory optimization for motion planning, in: *IEEE international conference on robotics and automation*, 2011, pp. 4569–4574.
- [8] K. J. Åström, *Introduction to stochastic control theory*, Courier Corporation, 2012.
- [9] S. Thrun, Probabilistic robotics, *Communications of the ACM* 45 (3) (2002) 52–57.
- [10] M. Mukadam, X. Yan, B. Boots, Gaussian process motion planning, in: *IEEE international conference on robotics and automation (ICRA)*, 2016, pp. 9–15.
- [11] M. Mukadam, J. Dong, X. Yan, F. Dellaert, B. Boots, Continuous-time gaussian process motion planning via probabilistic inference, *The International Journal of Robotics Research* 37 (11) (2018) 1319–1340.
- [12] M. D. Hoffman, D. M. Blei, C. Wang, J. Paisley, Stochastic variational inference, *Journal of Machine Learning Research* (2013).
- [13] D. M. Blei, A. Kucukelbir, J. D. McAuliffe, Variational inference: A review for statisticians, *Journal of the American Statistical Association* 112 (518) (2017) 859–877.
- [14] H. Yu, Y. Chen, A gaussian variational inference approach to motion planning, *IEEE Robotics and Automation Letters* 8 (5) (2023) 2518–2525.
- [15] H. Yu, Y. Chen, Stochastic motion planning as gaussian variational inference: Theory and algorithms, *arXiv preprint arXiv:2308.14985* (2023).
- [16] L. C. Cosier, R. Iordan, S. N. Zwane, G. Franzese, J. T. Wilson, M. Deisenroth, A. Terenin, Y. Bekiroglu, A unifying variational framework for gaussian process motion planning, in: *International Conference on Artificial Intelligence and Statistics*, PMLR, 2024, pp. 1315–1323.
- [17] T. Power, D. Berenson, Constrained stein variational trajectory optimization, *IEEE Transactions on Robotics* (2024).
- [18] D. Hsu, L. E. Kavraki, J.-C. Latombe, R. Motwani, S. Sorkin, et al., On finding narrow passages with probabilistic roadmap planners, in: *Robotics: the algorithmic perspective: 1998 workshop on the algorithmic foundations of robotics*, 1998, pp. 141–154.
- [19] Y. Chen, T. T. Georgiou, M. Pavon, On the relation between optimal transport and schrödinger bridges: A stochastic control viewpoint, *Journal of Optimization Theory and Applications* 169 (2016) 671–691.
- [20] Y. Chen, T. T. Georgiou, M. Pavon, Optimal transport over a linear dynamical system, *IEEE Transactions on Automatic Control* 62 (5) (2016) 2137–2152.
- [21] T. Haarnoja, A. Zhou, P. Abbeel, S. Levine, Soft actor-critic: Off-policy maximum entropy deep reinforcement learning with a stochastic actor, in: *International conference on machine learning*, Pmlr, 2018, pp. 1861–1870.
- [22] R. Zhao, X. Sun, V. Tresp, Maximum entropy-regularized multi-goal reinforcement learning, in: *International Conference on Machine Learning*, PMLR, 2019, pp. 7553–7562.
- [23] T. D. Barfoot, C. H. Tong, S. Särkkä, Batch continuous-time trajectory estimation as exactly sparse gaussian process regression., in: *Robotics: Science and Systems*, Vol. 10, Citeseer, 2014, pp. 1–10.
- [24] T. D. Barfoot, J. R. Forbes, D. J. Yoon, Exactly sparse gaussian variational inference with application to derivative-free batch nonlinear state estimation, *The International Journal of Robotics Research* 39 (13) (2020) 1473–1502.
- [25] M. E. E. Khan, P. Baqué, F. Fleuret, P. Fua, Kullback-leibler proximal variational inference, *Advances in neural information processing systems* 28 (2015).
- [26] M. E. Khan, R. Babanezhad, W. Lin, M. Schmidt, M. Sugiyama, Faster stochastic variational inference using proximal-gradient methods with general divergence functions, *arXiv preprint arXiv:1511.00146* (2015).

- [27] O. Shental, P. H. Siegel, J. K. Wolf, D. Bickson, D. Dolev, Gaussian belief propagation solver for systems of linear equations, in: *IEEE International Symposium on Information Theory*, 2008, pp. 1863–1867.
- [28] J. Ortiz, T. Evans, A. J. Davison, A visual introduction to gaussian belief propagation, *arXiv preprint arXiv:2107.02308* (2021).
- [29] T. Osa, Multimodal trajectory optimization for motion planning, *The International Journal of Robotics Research* 39 (8) (2020) 983–1001.
- [30] S. Särkkä, A. Solin, *Applied stochastic differential equations*, Vol. 10, Cambridge University Press, 2019.
- [31] F. Dellaert, Factor graphs: Exploiting structure in robotics, *Annual Review of Control, Robotics, and Autonomous Systems* 4 (1) (2021) 141–166.
- [32] T. D. Barfoot, *State estimation for robotics*, Cambridge University Press, 2024.
- [33] M. Z. Diao, K. Balasubramanian, S. Chewi, A. Salim, Forward-backward gaussian variational inference via jko in the bures-wasserstein space, in: *International Conference on Machine Learning*, PMLR, 2023, pp. 7960–7991.
- [34] A. Gelb, et al., *Applied optimal estimation*, MIT press, 1974.
- [35] S. J. Julier, J. K. Uhlmann, New extension of the kalman filter to nonlinear systems, in: *Signal processing, sensor fusion, and target recognition VI*, Vol. 3068, Spie, 1997, pp. 182–193.
- [36] I. Arasaratnam, S. Haykin, Cubature kalman filters, *IEEE Transactions on automatic control* 54 (6) (2009) 1254–1269.
- [37] K. Ito, K. Xiong, Gaussian filters for nonlinear filtering problems, *IEEE transactions on automatic control* 45 (5) (2000) 910–927.
- [38] D. Henrich, Fast motion planning by parallel processing—a review, *Journal of Intelligent and Robotic Systems* 20 (1997) 45–69.
- [39] R. Duncan, A survey of parallel computer architectures, *Computer* 23 (2) (1990) 5–16.
- [40] Y. Zhou, J. Zeng, Massively parallel a* search on a gpu, in: *Proceedings of the AAAI conference on artificial intelligence*, Vol. 29, 2015.
- [41] A. Fukunaga, A. Botea, Y. Jinnai, A. Kishimoto, Parallel a* for state-space search, *Handbook of Parallel Constraint Reasoning* (2018) 419–455.
- [42] M. Kameyama, T. Amada, T. Higuchi, Highly parallel collision detection processor for intelligent robots, *IEEE journal of solid-state circuits* 27 (4) (1992) 500–506.
- [43] J. Pan, D. Manocha, Gpu-based parallel collision detection for fast motion planning, *The International Journal of Robotics Research* 31 (2) (2012) 187–200.
- [44] P. Hyatt, C. S. Williams, M. D. Killpack, Parameterized and gpu-parallelized real-time model predictive control for high degree of freedom robots, *arXiv preprint arXiv:2001.04931* (2020).
- [45] I. V. Girsanov, On transforming a certain class of stochastic processes by absolutely continuous substitution of measures, *Theory of Probability & Its Applications* 5 (3) (1960) 285–301.
- [46] H. Yu, D. F. Franco, A. M. Johnson, Y. Chen, Optimal covariance steering of linear stochastic systems with hybrid transitions, *arXiv preprint arXiv:2410.13222* (2024).
- [47] N. Parikh, S. Boyd, et al., Proximal algorithms, *Foundations and trends® in Optimization* 1 (3) (2014) 127–239.
- [48] J. Altosaar, R. Ranganath, D. Blei, Proximity variational inference, in: *International Conference on Artificial Intelligence and Statistics*, PMLR, 2018, pp. 1961–1969.
- [49] S. Chrétien, A. O. Hero, Kullback proximal algorithms for maximum-likelihood estimation, *IEEE transactions on information theory* 46 (5) (2000) 1800–1810.
- [50] I. Arasaratnam, S. Haykin, R. J. Elliott, Discrete-time nonlinear filtering algorithms using gauss–hermite quadrature, *Proceedings of the IEEE* 95 (5) (2007) 953–977.
- [51] T. Gerstner, M. Griebel, Numerical integration using sparse grids, *Numerical algorithms* 18 (3) (1998) 209–232.
- [52] B. Jia, M. Xin, Y. Cheng, Sparse gauss-hermite quadrature filter with application to spacecraft attitude estimation, *Journal of Guidance, Control, and Dynamics* 34 (2) (2011) 367–379.
- [53] F. Heiss, V. Winschel, Likelihood approximation by numerical integration on sparse grids, *Journal of Econometrics* 144 (1) (2008) 62–80.
- [54] B. Rooks, The harmonious robot, *Industrial Robot: An International Journal* 33 (2) (2006) 125–130.
- [55] W. Garage, *Pr2 user manual* (2012).
- [56] M. Quigley, K. Conley, B. Gerkey, J. Faust, T. Foote, J. Leibs, R. Wheeler, A. Y. Ng, et al., Ros: an open-source robot operating system, in: *ICRA workshop on open source software*, Vol. 3, Kobe, 2009, p. 5.
- [57] D. Coleman, I. Sucan, S. Chitta, N. Correll, Reducing the barrier to entry of complex robotic software: a moveit! case study, *arXiv preprint arXiv:1404.3785* (2014).